DOI 10.59277/RoAJ.2023.1-2.10

# DIFFERENT EFFECTS OF PERTURBATIONS (SOLAR SAIL) ON THE MOTION OF THE TEST PARTICLES IN CR3BP

ABDULLAH

*Department of Mathematics, Dyal Singh College,*
*University of Delhi, New Delhi, India,*
Email*: abdullah.maths@dsc.du.ac.in*

*Abstract.* The idea of solar sail is used to investigate the motion properties of the test particle which is varying its mass according to the Jeans law and moving under the gravitational forces of the primaries, the Coriolis and centrifugal forces in the circular restricted three-body system (CRTBS). The equations of motion of the test particle are determined under the above said perturbations. And hence, the dynamical properties like the locations of equilibrium points, their stability, periodic orbits, Poincaré surfaces of section and basins of attracting domain are investigated. This problem will help those researchers who are interested in studying the problem related to solar sail for space missions.

*Key words*: solar sail, oblateness, variable mass, clock angle.

## 1. INTRODUCTION

Important features of the test particle can be discussed with various perturbing parameters in the restricted problem either the configuration contains three-body or more. The perturbation parameters can also be supposed from either natural or artificial. These parameters separately play an important role on the motion of the test particle. Researchers have investigated their problems by assuming either natural, artificial or both perturbing parameters. Solar sail, shapes of the bodies, variable mass, coriolis and centrifugal forces are few of the perturbations. Some of those researchers who have studied these perturbations are as follows:

Bhatnagar and Hallan (1978) have studied the effects of coriolis and centrifugal forces on the stability of equilibrium points in the restricted three-body problem. McInnes and Simmons (1992a,b) have studied the motion properties in geocentric and heliocentric cases with solar sail which perform minimum and families of linearly stable trajectories identified. After patching these halo orbits, new complex trajectories were found. McInnes *et al.* (1994) have evaluated the stationary solutions to the restricted three-body problem for the solar sail spacecraft in both Earth-Sun and Earth-moon systems. They observed that stationary solutions are unstable therefore they developed a simple closed-loop control scheme to ensure asymptotic stability. McInnes (2000) have studied the solar sail mission design in the circular restricted three-body problem with various strategies.

McInnes *et al.* (2001) have explored the geomagnetic tail using the small solar sail, because solar sails do not require reaction mass, a geomagnetic tail mission can be configured so that it provides a continuous science return by permanently stationing a science pay load within the geomagnetic tail. Mengali *et al.* (2007) have proposed a refined mathematical model for describing the acceleration exerted by solar sail. They also elaborated on how the main variable affects to the force coefficients. Macdonald *et al.* (2007) have examined the solar sail magnetotail mission concept. Using a parametric analysis, they identified the key sail technology requirements. Farrés (2009) have investigated the effects of solar sail on the motion properties (like families of equilibrium points, stability of equilibrium points, station keeping strategies and periodic orbits) of infinitesimal bodies in the restricted three-bodies.

Farrés and Jorba (2010) have considered the Earth-Sun restricted three-body model to investigate the effects of solar sail. For different values of the orientations of the solar sail, they have explained the periodic and quasi-periodic motions of a solar sail close to equilibrium points that lies between the Earth and the Sun. Gong and Li (2014) have investigated the solar sail with a reflection control device in the Heliocentric elliptic displaced orbits. They found the stable orbits in the pulsating rotating frame and imaged the polar region of the planet with an orbit that is highly elliptic. Heiligers, Mingotti, and McInnes (2015) have investigated the time-optimal solar sail transfers trajectories in two cases *i.e.* 1. Libration point orbits (LPOs) of Sun-Earth $L_2$-Halo orbit to Sun-Mars $L_1$-Halo orbit, 2. Libration point orbits (LPOs) of Sun-Earth $L_1$-Halo orbit to Sun-Mercury $L_2$-Halo orbit.

Peloni, Ceriotti, and Dachwald (2016) have presented a method to find sequences of encounters for multiple Near-Earth-Asteroid rendezvous missions by solar sailing. They also have demonstrated the novel coplanar shape-based approach for solar sailing to obtain excellent results both within the sequence search and as an initial-guess solution for 3D direct optimization. Sood and Howell (2019) have re-evaluated the concept of a mission to $L_{4,5}$ in the restricted three-body problem with solar sail dynamics. Singh *et al.* (2022) have investigated the effects of modified newtonian force on the restricted three-body configuration in non-linear sense.

After proper transformations, scales and limit in the restricted problem, the new type of problem that is generated is known as Hill problem. Many Mathematicians and Physicists have illustrated the Hill problems with various factors. Some of them are as follow: Szebehely (1967), Abouelmagd and El-Shaboury (2012), Alshaery and Abouelmagd (2020), Abouelmagd *et al.* (2022).

Ansari (2017, 2018); Ansari, Alhusain, and Kellil (2019); Ansari and Prasad (2020), Sahdev and Ansari (2020), Bouaziz and Ansari (2021), Ansari and Abouelmagd (2021); Ansari, Kellil, and Sahdev (2022), Albidah and Abdullah (2023b); Albidah, Abdullah, and Kellil (2023); Albidah and Abdullah (2023a) have investigated

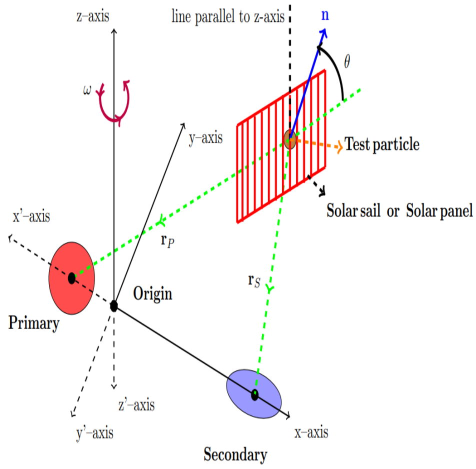


Fig. 1 – Presentation of the restricted 3-body problem with solar sail.

the effect of mass variation in the restricted system. They obtained that due to mass variation effects, all the equilibrium points become unstable while in the classical case (constant mass case), there are three unstable collinear equilibrium points and two stable triangular equilibrium points. They also illustrated these models numerically for location of equilibrium points, their stability, regions of motion, Poincaré surfaces of section, periodic orbits and basins of attraction.

From the space technology grand challenges, we got the motivation to study the restricted three-body problem with different effects of perturbations as the solar sail, mass variation effects, coriolis and centrifugal forces. To manage in-space resources, solar sail can be used as an alternative source of energy. Therefore, this study will be useful for readers who are interested to study the motion of solar sail spacecrafts in the Earth-Moon system.

The distribution of sections and subsections in this manuscript are as follows: The introduction of the problem is presented in Section 1. The geometrical presentation and the equations of motion are given in Section 2. Section 3 represents the numerical investigation of the problem with many subsections. The manuscript ends with conclusion in Section 4.

## 2. GEOMETRICAL PRESENTATION AND EQUATIONS OF MOTION

Let there be three masses $m_1$, $m_2$ and $m$ of primary, oblate secondary and the variable mass test particle respectively. The solar sail is considered on the test particle. The primary and secondary are placed at $x$-axis on either side of the origin and moving around their common center of mass which is taken as origin. The perpendicular line of x-axis is taken as y-axis and the perpendicular line of the xy-plane is considered as z-axis which have angular velocity $\omega$. The effects of coriolis as well as centrifugal forces are considered. $r_P$ and $r_S$ are the distances from primary and oblate secondary (with oblateness factor A) to the test particle respectively. Figure 1 represents the complete view of the problem. Using the procedures given by Farrés, Heiligers, and Miguel (2019) and Abouelmagd and Mostafa (2015), one can write the equations of motion of the test particle by assuming that it has zero momenta and originate from one point as:

$$\begin{aligned}
\frac{\dot{m}}{m}(\dot{x}-\delta_1\,\omega\,y) &+ \ddot{x}-2\,\delta_1\,\omega\,\dot{y} = \frac{\partial\mathbf{S}}{\partial x} + S_1,\\
\frac{\dot{m}}{m}(\dot{y}+\delta_1\,\omega\,x) &+ \ddot{y}+2\,\delta_1\,\omega\,\dot{x} = \frac{\partial\mathbf{S}}{\partial y} + S_2,\\
\frac{\dot{m}}{m}\dot{z} &+ \ddot{z} = \frac{\partial\mathbf{S}}{\partial z} + S_3,
\end{aligned} \tag{1}$$

with

$$\begin{aligned}
\mathbf{S} &= \frac{\delta_2\,\omega^2}{2}(x^2+y^2)+\frac{1-\mu}{r_P}+\frac{\mu}{r_S}+\frac{A\,\mu}{2\,r_S^3},\\
S_1 &= B\left[\frac{x+\mu}{r_P}\,cos\,\theta-\frac{(x-\mu)\,z}{r_1\,r_P}\,sin\,\theta\cdot cos\,\phi+\frac{y}{r_1}\,sin\,\theta\cdot sin\,\phi\right],\\
S_2 &= B\left[\frac{y}{r_P}\,cos\,\theta-\frac{y\,z}{r_1\,r_P}\,sin\,\theta\cdot cos\,\phi-\frac{x-\mu}{r_1}\,sin\,\theta\cdot sin\,\phi\right],\\
S_3 &= B\left[\frac{z}{r_P}\,cos\,\theta+\frac{r_1}{r_P}\,sin\,\theta\cdot cos\,\phi\right],\\
B &= \frac{q(1-\mu)}{m\,r_P^2}\cdot cos^2\,\theta,\quad r_P^2=(x+\mu)^2+y^2+z^2,\\
r_S^2 &= (x+\mu-1)^2+y^2+z^2,\quad r_1^2=(x-\mu)^2+y^2,\\
\mu &= \frac{m_2}{m_1+m_2},\quad \omega^2=1+\frac{3}{2}A,\quad A = \text{the oblateness parameter},
\end{aligned}$$

$\theta$ = pitch angle $\in [-\frac{\pi}{2}, \frac{\pi}{2}]$, $q =$ the radiation parameter per unit mass,

$\phi$ = clock angle $\in [0, \pi]$, the vector n can not point in direction of Sun,

$\delta_1$ & $\delta_2$ = coriolis and centrifugal forces parameters respectively.

and also $S$ is the potential function without solar sail, $S_1, S_2$ and $S_3$ are the forces on the test particle due to solar sail in the $x$, $y$ and $z$ direction respectively. $B$ is the part of $S_1, S_2$ and $S_3$ including radiation parameter.

The test particle varies its mass therefore to simplify Eq. (1), we will use Jean's law Jeans (1928) and Meshcherskii space-time transformations Meshcherskii (1949) as:

$$m = m_0 e^{-\epsilon_1 t} \text{ and } (x, y, z) = \epsilon_2^{-1/2} (\xi, \eta, \zeta). \tag{2}$$

where $\epsilon_1$ is variation constant and $\epsilon_2 = \frac{m}{m_0}$, where $m_0$ is the initial mass. From Eqs. (1) and (2), we obtain:

$$\begin{aligned} \ddot{\xi} - 2\delta_1 \omega \dot{\eta} &= \frac{\partial \mathbf{S_v}}{\partial \xi} + S_{v_1}, \\ \ddot{\eta} + 2\delta_1 \omega \dot{\xi} &= \frac{\partial \mathbf{S_v}}{\partial \eta} + S_{v_2}, \\ \ddot{\zeta} &= \frac{\partial \mathbf{S_v}}{\partial \zeta} + S_{v_3}, \end{aligned} \tag{3}$$

with

$$\mathbf{S_v} = \frac{\epsilon_1^2}{8}(\xi^2 + \eta^2 + \zeta^2) + \frac{\delta_2 \omega^2}{2}(\xi^2 + \eta^2) + \epsilon_2^{3/2} \left\{ \frac{1-\mu}{\rho_P} + \frac{\mu}{\rho_S} + \frac{A \mu \epsilon_2}{2 \rho_S^3} \right\},$$

$$S_{v_1} = B_0 \sqrt{\epsilon_2} \left[ \frac{\xi + \mu\sqrt{\epsilon_2}}{\rho_P} cos\,\theta - \frac{(\xi - \mu\sqrt{\epsilon_2})\,\zeta}{\rho_1 \rho_P} sin\,\theta \cdot cos\,\phi + \frac{\eta}{\rho_1} sin\,\theta \cdot sin\,\phi \right],$$

$$S_{v_2} = B_0 \sqrt{\epsilon_2} \left[ \frac{\eta}{\rho_P} cos\,\theta - \frac{\eta\,\zeta}{\rho_1 \rho_P} sin\,\theta \cdot cos\,\phi - \frac{\xi - \mu\sqrt{\epsilon_2}}{\rho_1} sin\,\theta \cdot sin\,\phi \right],$$

$$S_{v_3} = B_0\sqrt{\epsilon_2}\left[\frac{\zeta}{\rho_P}\,cos\,\theta + \frac{\rho_1}{\rho_P}\,sin\,\theta\cdot cos\,\phi\right], \quad q_0 = \frac{q}{m_0} << 1,$$

$$B_0 = \frac{q_0(1-\mu)}{\rho_P^2}\cdot cos^2\,\theta, \quad \rho_P^2 = (\xi+\mu\sqrt{\epsilon_2})^2+\eta^2+\zeta^2,$$

$$\rho_S^2 = (\xi+(\mu-1)\sqrt{\epsilon_2})^2+\eta^2+\zeta^2, \quad \rho_1^2 = (\xi-\mu\sqrt{\epsilon_2})^2+\eta^2.$$

## 3. NUMERICAL INVESTIGATION

We will investigate numerically the dynamical properties of the test particle as the locations of equilibrium points, their stability, periodic orbits, Poincaré surfaces of section and basins of attracting domain in various subsections.

### 3.1. EQUILIBRIUM POINTS

Equilibrium points are the place where the test particle can park. To determine the locations of equilibrium points, we will put zero to all the derivatives with respect to time in the Eq. (3), and hence we obtain:

$$\begin{aligned} \mathbf{S}_{\mathbf{v}_\xi} &+ S_{v_1} = 0,\\ \mathbf{S}_{\mathbf{v}_\eta} &+ S_{v_2} = 0,\\ \mathbf{S}_{\mathbf{v}_\zeta} &+ S_{v_3} = 0. \end{aligned} \tag{4}$$

When we contour plot with the first two lines of Eqs. (4) numerically in Mathematica software with numerical values $z=0$, $\mu=0.01215$, $\delta_1=\delta_2=1.2$, $A=0.001$, $q=0.2$, we obtain the locations of equilibrium points. These equilibrium points are known as in-plane equilibrium points. When we contour plot with the first and third lines of Eq. (4) numerically with numerical values $y=0$, $\mu=0.01215$, $\delta_1=\delta_2=1.2$, $A=0.001$, $q=0.2$, we obtain the locations of equilibrium points. These equilibrium points are known as out-of-plane equilibrium points.

Here, we have presented the in-plane equilibrium points only. These equilibrium points are given in Figures 2, 3 and 4. Figures 2 and 3 represent the equilibrium points in constant mass case for the different values of $\theta$ and $\phi$, while Figure 4 represents the equilibrium points in variable mass case for the different values of $\theta$ and $\phi$. From Figure 2, we observed that for various values of $\phi$ and two values of $\theta(=0,\pi/2)$, there exist five equilibrium points as for classical case of the restricted three-body problem.

From Figure 3, we observed that for $\theta = \pi/4$ and $\phi = 0, \pi$, there exist five equilibrium points, while for the same $\theta$ and the other values of $\phi(= \pi/2, 3\pi/4)$, there exist only three equilibrium points. From Figure 4, we observed the same pattern as in Figure 3, the difference is just that here the locations of equilibrium points are shrinking. In these figures the black dots are the locations of equilibrium points. Here we also observed that equilibrium points are not affected by coriolis force.

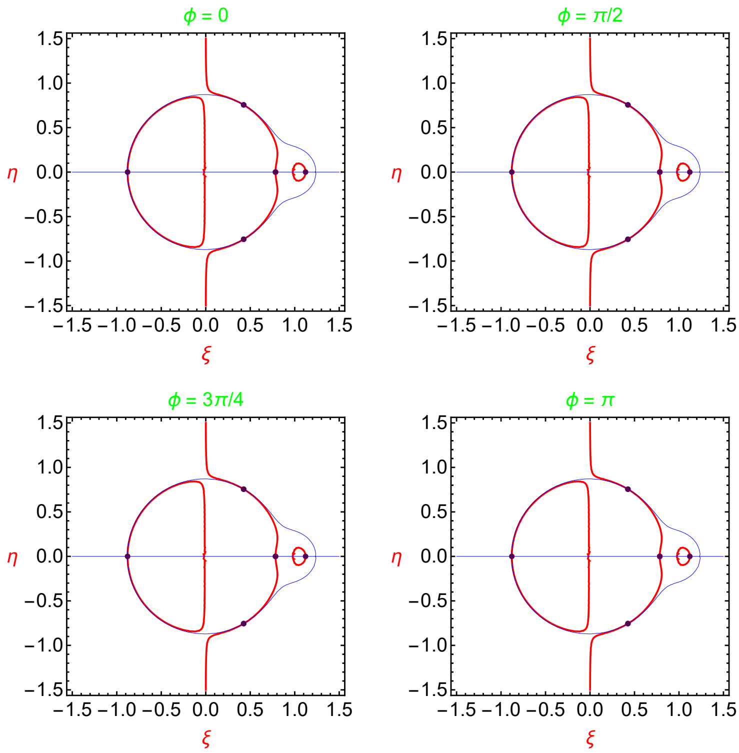


Fig. 2 – Locations of equilibrium points for $\theta = 0, \pi/2$, $\epsilon_1 = 0$ and $\epsilon_2 = 1$.

### 3.2. STABILITY STATES

To examine the stability of equilibrium points, we will follow the procedure given by Zhang, Zhao, and Xiong (2012). And hence the characteristic polynomial corresponding to equation (3) can be written as:

$$f(\lambda) = P_6\lambda^6 + P_5\lambda^5 + P_4\lambda^4 + P_3\lambda^3 + P_2\lambda^2 + P_1\lambda + P_0, \tag{5}$$

where:

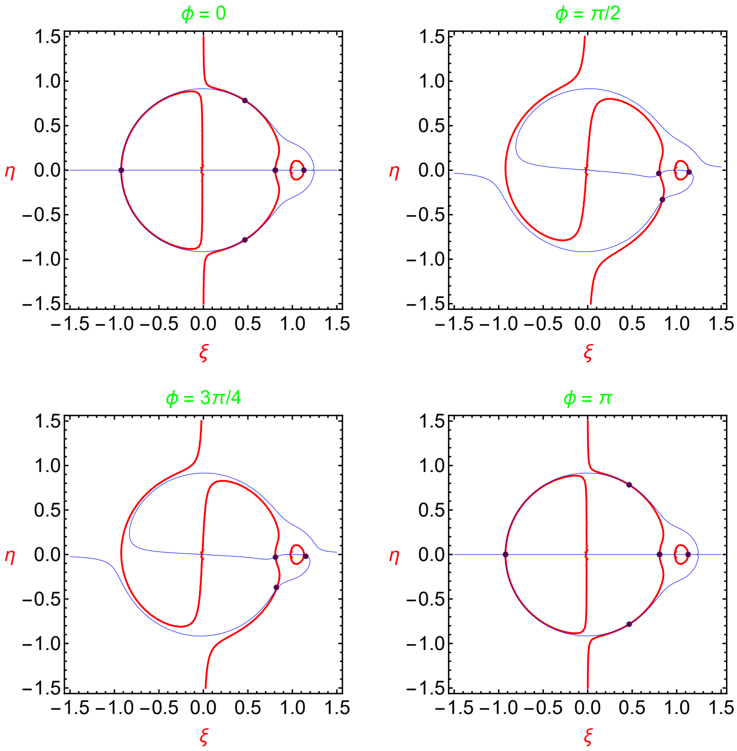


Fig. 3 – Locations of equilibrium points for $\theta = \pi/4$, $\epsilon_1 = 0$ and $\epsilon_2 = 1$.

$$
\begin{aligned}
\Gamma_\xi &= \mathbf{S}_{\mathbf{v}_\xi} + S_{v_1},\\
\Gamma_\eta &= \mathbf{S}_{\mathbf{v}_\eta} + S_{v_2},\\
\Gamma_\zeta &= \mathbf{S}_{\mathbf{v}_\zeta} + S_{v_3},\\
P_6 &= 1,\\
P_5 &= -3\,\epsilon_1\\
P_4 &= \frac{15}{4}\,\epsilon_1^2 + 4\,\delta_1^2\,\omega^2 - (\Gamma_{\xi\xi} + \Gamma_{\eta\eta} + \Gamma_{\zeta\zeta}),\\
P_3 &= -\frac{5}{2}\,\epsilon_1^3 - 8\,\delta_1^2\,\epsilon_1\,\omega^2 + 2\,\epsilon_1\,(\Gamma_{\xi\xi} + \Gamma_{\eta\eta} + \Gamma_{\zeta\zeta}),\\
P_2 &= \frac{1}{16}\{15\,\epsilon_1^4 + 96\,\delta_1^2\,\epsilon_1^2\,\omega^2 - 24\,\epsilon_1^2\,(\Gamma_{\xi\xi} + \Gamma_{\eta\eta} + \Gamma_{\zeta\zeta}) - 64\delta_1^2\,\omega^2\,\Gamma_{\zeta\zeta}\\
&\quad + 16(\Gamma_{\xi\xi}\,\Gamma_{\eta\eta} + \Gamma_{\xi\xi}\,\Gamma_{\zeta\zeta} + \Gamma_{\eta\eta}\,\Gamma_{\zeta\zeta} - \Gamma_{\xi\eta}^2)\},\\
P_1 &= \frac{1}{16}\{-3\,\epsilon_1^5 - 32\,\delta_1^2\,\epsilon_1^3\,\omega^2 + 8\,\epsilon_1^3\,(\Gamma_{\xi\xi} + \Gamma_{\eta\eta} + \Gamma_{\zeta\zeta}) + 64\delta_1^2\,\omega^2\,\epsilon_1\,\Gamma_{\zeta\zeta}\\
&\quad - 16\,\epsilon_1\,(\Gamma_{\xi\xi}\,\Gamma_{\eta\eta} + \Gamma_{\xi\xi}\,\Gamma_{\zeta\zeta} + \Gamma_{\eta\eta}\,\Gamma_{\zeta\zeta} + \Gamma_{\xi\eta}^2)\},\\
P_0 &= \frac{1}{64}\{\epsilon_1^6 + 16\,\delta_1^2\,\epsilon_1^4\,\omega^2 - 4\,\epsilon_1^4\,(\Gamma_{\xi\xi} + \Gamma_{\eta\eta} + \Gamma_{\zeta\zeta})\\
&\quad - 64\,\Gamma_{\zeta\zeta}\,(\delta_1^2\,\omega^2\,\epsilon_1^2 + \Gamma_{\xi\xi}\,\Gamma_{\eta\eta} - \Gamma_{\xi\eta}^2)\\
&\quad + 16\,\epsilon_1^2\,(\Gamma_{\xi\xi}\,\Gamma_{\eta\eta} + \Gamma_{\xi\xi}\,\Gamma_{\zeta\zeta} + \Gamma_{\eta\eta}\,\Gamma_{\zeta\zeta} - \Gamma_{\xi\eta}^2)\}.
\end{aligned}
\tag{6}
$$

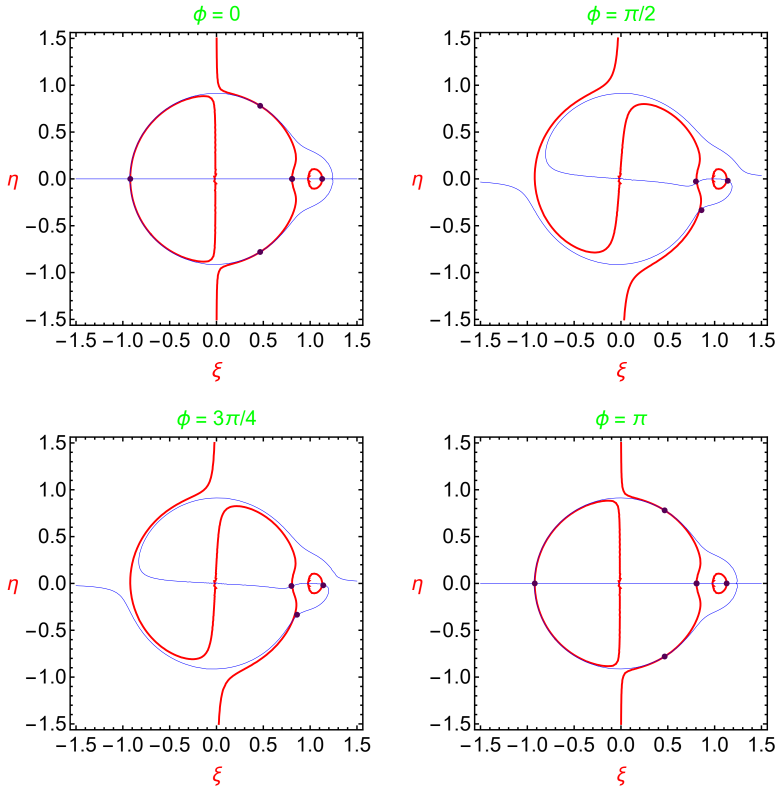


Fig. 4 – Locations of equilibrium points for $\theta = \pi/4$, $\epsilon_1 = 0.2$ and $\epsilon_2 = 0.4$.

We have numerically solve Eq. (5) corresponding to equilibrium points for the various values of the parameters used and mentioned in Table 1. From this table, we got at least one root is positive real value or positive real part of the complex roots. Hence these equilibrium points are unstable.

### 3.3. PERIODIC ORBITS

Trajectory allocations are the important part of the motion properties of the test particle. To allocate the path of the test particle during the motion, we have to solve the determined equations of motion. For which firstly, we have to write the equations of motion in phase plane and then proper choice of the initial values as well as by any well known software, we have evaluated the solutions of the equations of motion. With the use of these solutions, we have illustrated the periodic orbits for constant mass as well as for variable mass with time periods 25.7, as well as 26.3 units, respectively, and given in Figure 5. We observed from Figure 5 that test particle takes more time and cover more area in the variable mass case than in the

*Table 1*

The nature of equilibrium points corresponding to Figure (4) for

$\mu = 0.01215$, $A = 0.001$, $q = 0.2$, $\theta = \pi/4$, $\delta_2 = 1.2$, $\epsilon_1 = 0.2$ and $\epsilon_2 = 0.4$

| *Clock Angle* $\phi$ | *Roots* | *Nature* |
|---|---|---|
| $0\,\&\,\pi$ | Positive real part | *Unstable* |
| $\frac{3\pi}{4}\,\&\,\frac{\pi}{2}$ | Positive real value | *Unstable* |

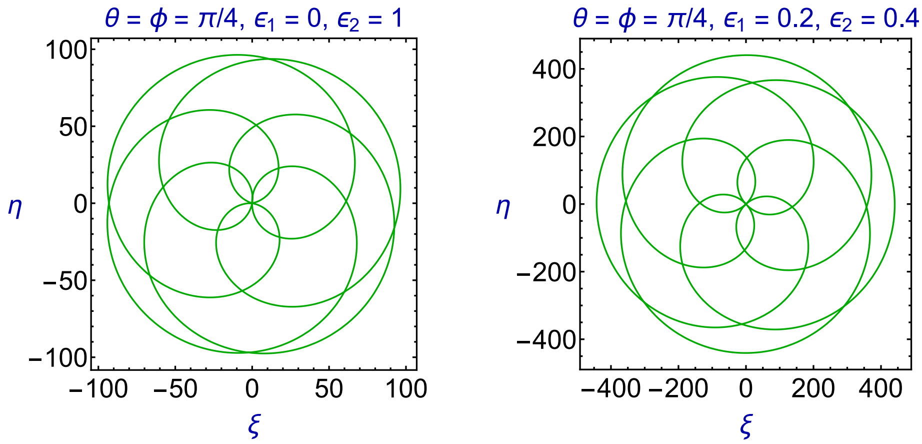


(a) For constant mass

(b) For variable mass

Fig. 5 – Periodic orbits in two cases.

constant mass case.

### 3.4. POINCARÉ SURFACES OF SECTION

The other name of Poincaré surfaces of section (PSS) is first return map by which one can observe the regularity or irregularity of the motion of the test particle. To illustrate the first return map, we have to determine the position $(\xi, \eta)$ and velocity $(\dot{\xi}, \dot{\eta})$ of the test particle in phase space. Then we draw the graph between $(\xi, \dot{\xi})$ at $\eta = 0$, whenever the path intersects the plane for $\dot{\eta} > 0$ and similarly can draw for $(\eta, , \dot{\eta})$. The plots of first return maps are given in Figures 6 and 7. Figure 6 is for the constant mass and Figure 7 is for variable mass. In both the cases there are much distortions which show chaos along both the axes.

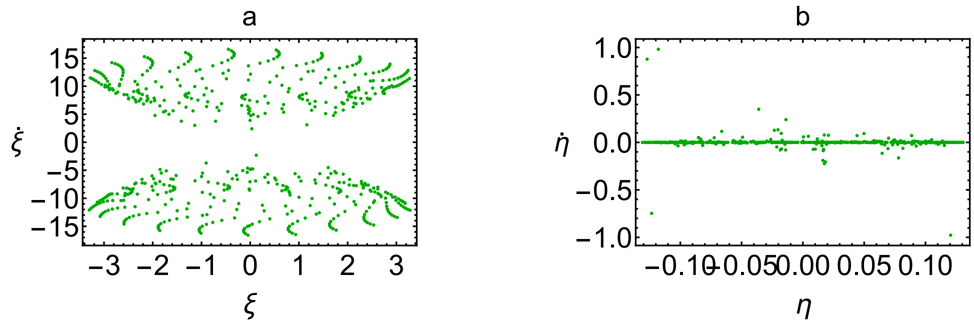


Fig. 6 – First return map for $\theta = \pi/4$, $\phi = \pi/4$, $\epsilon_1 = 0$ and $\epsilon_2 = 1$.

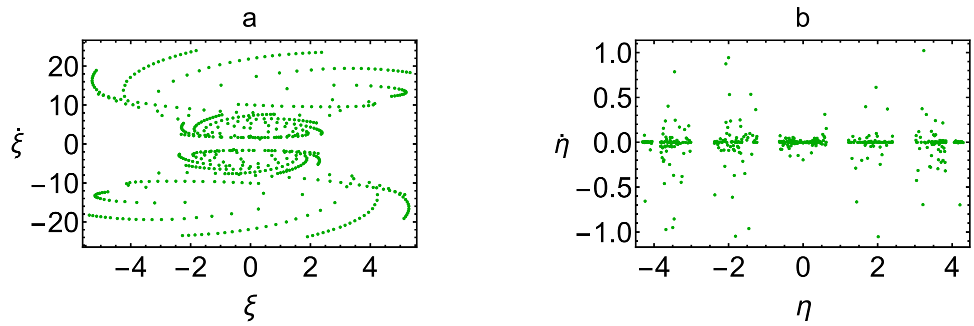


Fig. 7 – First return map for $\theta = \pi/4$, $\phi = \pi/4$, $\epsilon_1 = 0.2$ and $\epsilon_2 = 0.4$.

### 3.5. BASINS OF ATTRACTING DOMAIN

Basins of attracting domain is one of the interesting and important properties for the motion of test particle. It can be illustrated by the procedure given by Bouaziz and Ansari (2021). Here the equilibrium point acts as an attractor. Color code will be used for differentiating the regions. The algorithm for this problem is as follows:

$$\xi_{n+1} - \xi_n = -\left(\frac{\Gamma_\xi \times \Gamma_{\eta\eta} - \Gamma_\eta \times \Gamma_{\xi\eta}}{\Gamma_{\xi\xi} \times \Gamma_{\eta\eta} - \Gamma_{\xi\eta} \times \Gamma_{\eta\xi}}\right)_{(\xi_n,\eta_n)}, \tag{7}$$

$$\eta_{n+1} - \eta_n = -\left(\frac{\Gamma_\eta \times \Gamma_{\xi\xi} - \Gamma_\xi \times \Gamma_{\eta\xi}}{\Gamma_{\xi\xi} \times \Gamma_{\eta\eta} - \Gamma_{\xi\eta} \times \Gamma_{\eta\xi}}\right)_{(\xi_n,\eta_n)}, \tag{8}$$

where $\Gamma_\xi = \mathbf{S}_{\mathbf{v}_\xi} + S_{v_1}$, $\Gamma_\eta = \mathbf{S}_{\mathbf{v}_\eta} + S_{v_2}$, $\xi_n$ and $\eta_n$ are the values of $\xi$ and $\eta$ co-ordinates of the $n^{\text{th}}$ step of iterative process. The point $(\xi, \eta)$ will be a member of the attracting domain, if the initial point converges rapidly to one of the equilibrium points. This property of motion has been performed in constant mass case and variable mass case, these performances are given in Figure 8. In this figure black dots represent the locations of attracting points. The two attracting points are lie in

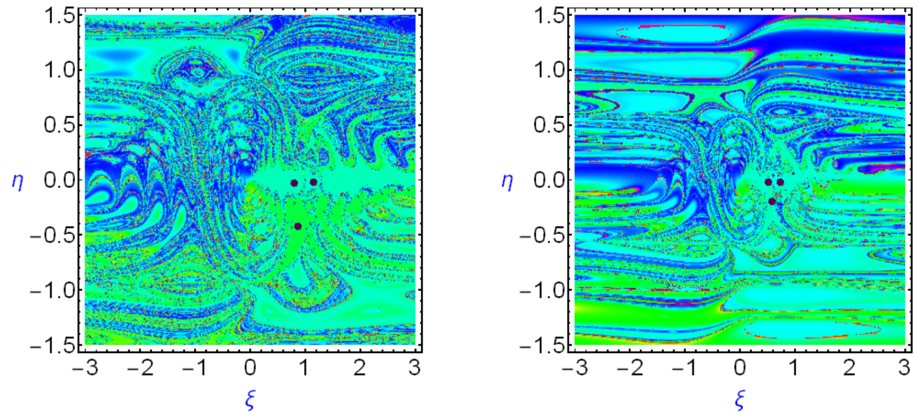


(a) $\epsilon_1 = 0$ and $\epsilon_2 = 1$

(b) $\epsilon_1 = 0.2$ and $\epsilon_2 = 0.4$

Fig. 8 – Basins of attracting domain.

the cyan region and one lies in the green region in both the cases and the patterns of the regions are same in color. The regions corresponding to attracting points are extended to infinity. The difference is only that in the variable mass case regions shrink.

## 4. CONCLUSION

The effect of solar sail on the motion of test particle have benn studied in the restricted three-body configuration. Where we have taken primary as spherical body, secondary as oblate body, test particle as variable mass body, the solar sail, the effects of coriolis and centrifugal forces. The equations of motion of the test particle clearly show the effects of these perturbations. With these determined equations of motion, we have numerically illustrated the dynamical properties (locations of equilibrium points, their stability, periodic orbits, Poincaré surfaces of section and basins of attracting domain) of the test particle motion. The locations of equilibrium points are found for different values of pitch and clock angle in the constant mass case and variable mass case. In both the cases, we observed that for the clock angle $\phi = 0, \pi$, there exist five equilibrium points while on the other values, there exist only three equilibrium points. It is also observed that the locations of equilibrium points are not affected by the coriolis force. After examine the stability, we found that all the equilibrium points are unstable. The subsection periodic orbits shown the periodic path with time period 25.7 and 26.3 units in both the cases. In the previous subsection, we illustrated the Poincaré surfaces of section and obtained some chaos in both the cases. In the basins of attracting domain, the equilibrium points act as attractors.

These attractors correspond to attracting regions which are extended to infinity here. In this way we observed the excellent influence of the solar sail and other perturbations on the motion of the test particle. This model will be helpful to those who want to study the space missions.

## CONFLICT OF INTEREST

The author declares no potential conflict of interests.

*Acknowledgements.* We are thankful to the anonymous editor and reviewer for their valuable suggestions. We are also thankful to the International center for advanced interdisciplinary research (ICAIR), New Delhi, India for providing the research facilities.

## REFERENCES

Abouelmagd, E.I., El-Shaboury, S.M.: 2012, Periodic orbits under combined effects of oblateness and radiation in the restricted problem of three bodies. *Astrophys. Space Sci.* **341**, 331 – 341.

Abouelmagd, E.I., Mostafa, A.: 2015, Out of plane equilibrium points locations and the forbidden movement regions in the restricted three-body problem with variable mass. *Astrophys. Space Sci.* **357**(58).

Abouelmagd, E.I., Alhowaity, S., Diab, Z., Guirao, J.L., Shehata, M.H.: 2022, On the periodic solutions for the perturbed spatial quantized hill problem. *Mathematics* **10**(4), 614.

Albidah, A., Abdullah: 2023a, Halo orbits under some perturbations in the cr3b problem. *Symmetry* **15**, 418.

Albidah, A., Abdullah: 2023b, Shapes and mass variation effects of the bodies in the generalized elliptic restricted 3-body problem. *Astronomy reports* **67**(4), 393 – 403.

Albidah, A., Abdullah, KellilR.: 2023, Interaction of 3-body in the circular restricted problem with variable mass. *Astronomy and computing* **42**.

Alshaery, A., Abouelmagd, E.I.: 2020, Analysis of the spatial quantized three-body problem. *Results in Physics* **17**, 103067.

Ansari, A.A.: 2017, Effect of albedo on the motion of the infinitesimal body in circular restricted three-body problem with variable masses. *Italian Journal Of Pure and Applied Mathematics* **38**, 581 – 600.

Ansari, A.A.: 2018, The circular restricted four- body problem with triaxial primaries and variable infinitesimal mass. *Applications and Applied Mathematics: An International Journal* **13**(2), 818 – 838.

Ansari, A.A., Prasad, S.N.: 2020, Generalized elliptic restricted four-body problem with variable mass. *Astron. Lett.* **46**, 275 – 288.

Ansari, A.A., Alhusain, Z.A., Kellil, R.: 2019, Behavior of an infinitesimal-variable-mass body in cr3bp; the primaries are finite straight segments. *Punjab University Journal of Mathematics* **51**(5), 107 – 120.

Ansari, A., Abouelmagd, E.: 2021, Variable mass motion in the hénon-heiles system. *Modern Physics Letters A* **36**(21).

Ansari, A., Kellil, R., Sahdev, S.: 2022, Numerical exploration of the variable mass test particle on the perturbed cr3b configuration. *New Astronomy* **97**(11), 101885.

Bhatnagar, K., Hallan, P.: 1978, Effect of perturbations in the coriolis and centrifugal forces on the stability of libration points in the restricted problem. *Celest. Mech. Dyn. Astron.* **18**, 105 – 112.

Bouaziz, F., Ansari, A.: 2021, Perturbed hill's problem with variable mass. *Astron. Nachr.*, 1 – 9.

Farrés, A., Heiligers, J., Miguel, N.: 2019, Road map to $l_4\,/\,l_5$ with a solar sail. *Aerospace Science and Technology* **95**, 105458.

Farrés, A.: 2009, Contribution to the dynamics of a solar sail in the earth-sun system. *PhD thesis, Universitat de Barcelona*.

Farrés, A., Jorba, A.: 2010, Periodic and quasi-periodic motions of a solar sail around the family $sl_1$ on the sun-earth system. *Celest. Mech. Dyn. Astron.* **107**, 233 – 253.

Gong, S., Li, J.: 2014, Solar sail heliocentric elliptic displaced orbits. *J. Guid. Control. Dyn.* **37**(64), 2021 – 2025.

Heiligers, J., Mingotti, G., McInnes, C.: 2015, Optimal solar sail transfers between halo orbits of different sun-planet systems. *Adv. Space Res.* **55**, 1405 – 1421.

Jeans, J.H.: 1928, Astronomy and Cosmogony. *Cambridge University Press, Cambridge*.

Macdonald, M., Hughes, G., McInnes, C., Lyngvi, A., Falkner, P., Atzei, A.: 2007, Geo-sail: an elegant solar sail demonstration mission. *J. Spacecraft and Rockets* **44**(6), 784 – 796.

McInnes, A.: 2000, Strategies for solar sail mission design in the circular restricted three-body problem. *Master's thesis, Purdue University* **August**.

McInnes, C., Simmons, J.: 1992a, Solar sail halo orbits i: Heliocentric case. *J. Spacecraft and Rockets* **29**(4), 466 – 471.

McInnes, C., Simmons, J.: 1992b, Solar sail halo orbits ii: Geocentric case. *J. Spacecraft and Rockets* **29**(4), 472 – 479.

McInnes, C., McDonald, A., Simmons, J., MacDonald, E.: 1994, Solar sail parking in restricted three-body system. *J. Guid. Control Dyn.* **17**(2), 399 – 406.

McInnes, C., MacDonald, M., Angelopolous, V., Alexander, D.: 2001, Geosail: Exploring the geomagnetic tail using a small solar sail. *J. Spacecraft and Rockets* **38**(4), 622 – 629.

Mengali, G., Quarta, A., Circi, C., Dachwald, B.: 2007, Refined solar sail force model with mission application. *J. Guid. Control Dyn.* **30**(2), 512 – 520.

Meshcherskii, I.V.: 1949, Works on the mechanics of bodies of variable mass. *GITTL, Moscow*.

Peloni, A., Ceriotti, M., Dachwald, B.: 2016, Solar-sail trajectory design for a multiple near-earth-asteroid rendezvous mission. *J. Guid. Control Dyn.* **39**, 2712 – 2724.

Sahdev, S., Ansari, A.: 2020, Various perturbations considered on the generalized circular restricted three-body problem. *Science International, Lahore* **32**(6), 771 – 776.

Singh, B., Shalini, K., Prasad, S., Ansari, A.: 2022, Study the effect of modified newtonian force on the restricted 3-body configuration in non-linear sense. *AAM: An Inter. Journal* **17**(2), 10.

Sood, R., Howell, K.: 2019, Solar sail transfers and trajectory design to sun-earth $l_4$, $l_5$; solar observations and potential earth trojan exploration. *The J. of the Astronautical Sciences*.

Szebehely, V.: 1967, Theory of orbits. *Academic Press, New York*.

Zhang, M.J., Zhao, C.Y., Xiong, Y.Q.: 2012, On the triangular libration points in photo-gravitational restricted three-body problem with variable mass. *Astrophys. Space Sci.* **337**, 107 – 113.

*Received on 25 July 2023*